Mixed metal nitride clusterfullerenes in cage isomers: LuxSc3−xN@C80 (x = 1, 2) as compared with MxSc3−xN@C80 (M = Er, Dy, Gd, Nd)

ARTICLE *in* THE JOURNAL OF PHYSICAL CHEMISTRY C · APRIL 2009

Impact Factor: 4.77 · DOI: 10.1021/jp9005263

4 AUTHORS, INCLUDING:

Shangfeng Yang
University of Science and Technology of Ch…
141 PUBLICATIONS **2,803** CITATIONS
SEE PROFILE

Alexey A Popov
Leibniz Institute for Solid State and Materia…
187 PUBLICATIONS **3,358** CITATIONS
SEE PROFILE

Mixed Metal Nitride Clusterfullerenes in Cage Isomers: $Lu_xSc_{3-x}N@C_{80}$ (x=1, 2) as Compared with $M_xSc_{3-x}N@C_{80}$ (M=Nd, Gd, Dy, Er)

Shangfeng Yang,[a,b] *Alexey A. Popov,*[b,c] *Chuanbao Chen,*[a] *and Lothar Dunsch**[b]

[a] Hefei National Laboratory for Physical Sciences at Microscale & Department of Materials Science and Engineering, University of Science and Technology of China (USTC), Hefei 230026, China

[b] Group of Electrochemistry and Conducting Polymers, Leibniz-Institute for Solid State and Materials Research (IFW) Dresden, D-01171 Dresden, Germany

[c] Department of Chemistry, Moscow State University, Leninskiye Gory, 119992 Moscow, Russia

* To whom correspondence should be addressed. E-mail: sfyang@ustc.edu.cn, l.dunsch@ifw-dresden.de.

RECEIVED DATE (to be automatically inserted after your manuscript is accepted if required according to the journal that you are submitting your paper to)

ABSTRACT: Two isomers of lutetium-scandium mixed metal nitride clusterfullerenes (MMNCFs) $Lu_xSc_{3-x}N@C_{80}$ (x=1, 2) have been synthesized and isolated for the first time and accordingly the interplay of the cluster structure and cage isomerism is followed. The electronic and vibrational properties of $Lu_xSc_{3-x}N@C_{80}$ (I, II, x=1, 2) are characterized by UV-vis-NIR and FTIR spectroscopies, respectively, revealing the effect of the composition of the encaged $Lu_xSc_{3-x}N$ cluster. A comparative study of $Lu_xSc_{3-x}N@C_{80}$ (I) with other $M_xSc_{3-x}N@C_{80}$ (I, M= Er, Dy, Gd, Nd) points to the dependence of their electronic and vibrational properties on the encaged metal. The cage structures of $Lu_xSc_{3-x}N@C_{80}$ (I, II, x=1, 2) are determined by ^{13}C NMR spectroscopy. The ^{45}Sc NMR spectroscopic study is carried out to probe the dynamics of the encaged Sc atoms. Finally DFT computations are used to address the effect of the composition of the encaged $Lu_xSc_{3-x}N$ cluster on the NMR lines and the structures of the $Lu_xSc_{3-x}N@C_{80}$ (I, II, x=1, 2) especially with respect to the carbon atoms.

KEYWORDS: nitride cluster compounds, endohedral fullerenes, lutetium, scandium NMR, UV-vis-NIR spectroscopy, vibrational spectroscopy.

Introduction

Metal nitride clusterfullerenes (NCFs) have been attracting great interest because of the feasibility of tuning the trapped metal atoms and of stabilizing a large variety of cage sizes including different isomeric structures.[1-6] In the NCF family, the mixed metal nitride clusterfullerenes (MMNCFs) which are NCFs with two or three different metals mixed in the encaged nitride cluster appear quite peculiar because their yield could be even higher than that of the homogeneous NCFs.[1,3,7-11] Such a noteworthy advantage makes MMNCFs a promising matrix to boost the yield of clusterfullerenes which might be low in NCFs for large metal ions. So far a number of MMNCFs have been isolated, including $MSc_2N@C_{80}$ (I_h) (M=Y, Ce, Gd, Tb, Er),[7,8,10-15] $M_2ScN@C_{80}$ (I_h) (M=Y, Gd, Er),[7,8,13,14] $ScYEr@C_{80}$ (I_h),[16] $Gd_xSc_{3-x}N@C_{80}$ (D_{5h}) (x=1, 2),[7] $DySc_2N@C_{76}$,[9] $MSc_2N@C_{68}$(M=Dy, Lu), and $Lu_2ScN@C_{68}$.[17] Very recently the first non-Scandium MMNCFs, $Lu_xY_{3-x}N@C_{80}$ (I) (x=1, 2), were also successfully isolated and the dependence of the pyramidalization of their carbon atoms on the encaged cluster was unfolded.[18] Note that so far the reports on the C_{80}:D_{5h}-based MMNCFs are limited to $Gd_xSc_{3-x}N@C_{80}$ (D_{5h}, x=1, 2) which we reported recently.[7] This is primarily caused by their lower yields compared to those of the C_{80}:I_h cage and the difficulties in their HPLC isolation since the NCFs with different cluster composition but the same carbon cage isomer often exhibit a very similar HPLC behaviour.[1,10,12]

The extensive studies on a series of homogenous NCFs $M_3N@C_{80}$ (I) (M=Y, Gd, Tb, Dy, Ho, Er, Tm) reveal that the ionic radius of the encaged metal, i.e., the size of the encaged M_3N cluster, plays the dominating role not only in the structure of the M_3N cluster in $M_3N@C_{80}$ (I) and the cluster-cage interaction but also in the yield and cage size distribution of the $M_3N@C_{2n}$ NCFs.[1,2,4,6] However, such dependences have not been

studied for MMNCFs yet despite of its importance on understanding the structure and stability of the MMNCFs.

In this paper we report on the synthesis and isolation of two isomers of Lu/Sc MMNCFs $Lu_xSc_{3-x}N@C_{80}$ (I, II, x=1, 2) and further apply them for a comparative study with other $M_xSc_{3-x}N@C_{80}$ (I, M=Er, Dy, Gd, Nd). Based on the intergrated peak areas of the HPLC chromatogram the relative yield of $Lu_xSc_{3-x}N@C_{80}$ (I, II, x=1, 2) to the corresponding homogenous MMNCFs $Lu_3N@C_{80}$ and $Sc_3N@C_{80}$ (I, II) is calculated. Detailed spectroscopic characterizations on the isolated $Lu_xSc_{3-x}N@C_{80}$ (I, II, x=1, 2) MMNCFs, including mass spectroscopic, UV-vis-NIR, FTIR and NMR spectroscopic studies, have been accomplished in order to determine their cage structures and to reveal their structural and electronic properties. DFT computations are also performed to address the effect of the composition of the encaged $Lu_xSc_{3-x}N$ cluster on the structures of the $Lu_xSc_{3-x}N@C_{80}$ (I, II, x=1, 2) especially with respect to the pyramidalization of carbon atoms. We also present a comparative study of $Lu_xSc_{3-x}N@C_{80}$ (I) with other $M_xSc_{3-x}N@C_{80}$ (I, M= Er, Dy, Gd, Nd) to reveal the dependence of their electronic and vibrational properties on the encaged metal.

Experimental Section

$Lu_xSc_{3-x}N@C_{80}$ (I, II, x=1, 2) are produced by a modified Krätschmer-Huffman DC-arc discharging method with the addition of NH_3 (20 mbar) as described elsewhere.[1,2,5,7-9,18] Briefly, a mixture of Lu_2O_3 and Sc_2O_3 (99.9%, MaTeck GmbH, Germany) and graphite powder was used (molar ratio of Lu:Sc:C=1:1:15). After DC-arc discharging, the soot was pre-extracted by acetone and further Soxhlet-extracted by CS_2 for 20 h. Fullerene isolation was performed by three-step HPLC. In the first step running in a

Hewlett-Packard instrument (series 1100), a linear combination of two analytical 4.6 × 250 mm Buckyprep columns (Nacalai Tesque, Japan) was applied with toluene as the eluent. The second and the third step isolations are performed by recycling HPLC (Sunchrom, Germany) using a semi-preparative 4.6 × 250 mm 5PYE or Buckyprep-M column (Nacalai Tesque, Japan) and toluene as the eluent. A UV detector set to 320 nm was used for fullerene detection for all steps. The purity of the isolated products was checked by laser desorption time-of-flight (LD-TOF) MS analysis running in both positive and negative ion modes (Biflex III, Bruker, Germany).

Sample preparation and experimental details for UV-Vis-NIR and FTIR spectroscopic measurements as well as DFT computations were described previously.[4,5,7-9] The 125 MHz ^{13}C and the 121.5 MHz ^{45}Sc NMR spectroscopic studies were performed in a multiprobe head PH 1152Z of an Avance 500 spectrometer (Bruker, Germany) at room temperature in carbon disulfide solutions with d_6-acetone as a lock.

Results and Discussion

Synthesis and isolation of the $Lu_xSc_{3-x}N@C_{80}$ (I, II, x=1, 2) MMNCFs: $Lu_xSc_{3-x}N@C_{80}$ (I, II, x=1, 2) MMNCFs were synthesized by the ''reactive gas atmosphere'' method.[1,2,5,7-9,18] A typical chromatogram of a $Lu_xSc_{3-x}@C_{2n}$ fullerene extract mixture obtained under the optimized condition (molar ratio of Lu:Sc:C=1:1:15) is shown in Figure 1, and for comparison those of other MMNCFs ($Gd_xSc_{3-x}N@C_{2n}$, $Dy_xSc_{3-x}N@C_{2n}$, $Lu_xY_{3-x}N@C_{2n}$) which we recently reported are also included in Figure 1.[7-9,17,18] According to the integrated area of the dominant fraction (t_{ret}: 31-37 min, see inset of Figure 1) in the HPLC chromatogram which corresponds to $Lu_xSc_{3-x}N@C_{80}$ (I, II, x=0-3), the sum yield of $Lu_xSc_{3-x}N@C_{80}$ reaches up to 95% of all the fullerenes.

Moreover, compared to other MMNCFs such as $Gd_xSc_{3-x}N@C_{2n}$, $Dy_xSc_{3-x}N@C_{2n}$, $Lu_xY_{3-x}N@C_{2n}$ which were synthesized under the similar conditions,[7-9,17,18] the sum yield of $Lu_xSc_{3-x}N@C_{80}$ (I, II, x=0-3) clearly surpasses those of the other three MMNCFs. This is understood by considering the effect of the size of the encaged metal ion as already revealed in many studies on homogenous NCFs.[1,2,4-9] Since Sc^{3+} and Lu^{3+} have significantly smaller ionic radii (0.75 and 0.85 Å, respectively) compared to those of Gd^{3+} (0.94 Å), Dy^{3+} (0.91 Å) and Y^{3+} (0.90 Å),[4,19] the yields of the homogenous Sc- and Lu-based NCFs are much higher than those of NCFs based on the other three metals,[3,4,5a,11,20] suggesting that Sc and Lu atoms have a higher tendency to be encaged within the fullerene cage. This reasonably facilitates the formation of the Lu/Sc MMNCFs.

The main products of the dominant fraction (fractions 1 and 2, see inset of Figure 1) are two isomers of $Lu_xSc_{3-x}N@C_{80}$ (I, II, x=0-3), which are isolated by a three-step HPLC (see Supporting Information S1). Briefly, in the first-step HPLC using a linear combination of two Buckyprep columns two mixed fractions (fractions 1 and 2) are collected, which are then subjected to the second-step HPLC isolation by a 5PYE or a Buckyprep column. In the third-step isolation, the four sub-fractions obtained in the second-tep isolation are isolated by recycling HPLC with different numbers of cycles, resulting in the successful isolations of eight products of $Lu_xSc_{3-x}N@C_{80}$ (I, II, x=0-3). They are identified by LD-TOF MS analysis (Figure 2) which confirms their high purity (≥ 99%) as well. [I think we should be careful here because it is only compositional purity, while isomeric purity certainly cannot be proved my mass-spectrometry…It could be proved because different fractions are obtained by multi-step HPLC and two products with the same m/Z are isolated from different fraction indicating the isomeric forms - SY]

The relative yields of $Lu_xSc_{3-x}N@C_{80}$ (I, II, x=0-3) have been calculated on the basis of the integrated areas of the corresponding chromatographic peaks in the last cycles of the third-step HPLC isolation (see Supporting Information S2). Under the optimized synthesis condition (molar ratio of Lu:Sc:C=1:1:15), the relative yield of the first isomer (isomer I) of $Lu_xSc_{3-x}N@C_{80}$ (x=0-3) is determined to be 1:2.5:2.7:1.4 ($Lu_3N@C_{80}$: $Lu_2ScN@C_{80}$: $LuSc_2N@C_{80}$: $Sc_3N@C_{80}$). Noteworthy, the yield of $Lu_2ScN@C_{80}$ (I) and $LuSc_2N@C_{80}$ (I) is 2.5 and 2.7 times of that of $Lu_3N@C_{80}$ (I) (ca. 1.8 and 1.9 times of that of $Sc_3N@C_{80}$ (I)), respectively, indicating the boosting effect of the yield of $Lu_xSc_{3-x}N@C_{80}$ (I) upon mixing Lu and Sc metals compared to the homogeneous Lu- and Sc-NCFs.[12] [(We have already discussed in ACIE paper that "the boosting effect" can be only a statistical distribution [ideal ratio is 1:3:3:1 of the products if the ratio of the metals is 1:1]; I think that to say anything meaningful about the "boosting effect", we should compare absolute yields in the synthesis of the homogeneous NCFs with the sum of yields of the mixed NCFs). This has been confirmed experimentally.-SY] This result is consistent with that obtained from other MMNCFs such as $Gd_xSc_{3-x}N@C_{2n}$, $Dy_xSc_{3-x}N@C_{2n}$, $Lu_xY_{3-x}N@C_{2n}$ which we reported earlier.[7-9,17,18] Nevertheless, comparing $Lu_2ScN@C_{80}$ (I) and $LuSc_2N@C_{80}$ (I), we note that their yield is quite comparable (~1:1.1). This is obviously different to the case of $Gd_xSc_{3-x}N@C_{80}$ (I, x=1, 2) for which the yield of $Gd_2ScN@C_{80}$ (I):$GdSc_2N@C_{80}$ (I) is 1:3.9.[7,8] This result reveals once more the strong influence of size of the metal ion on the formation of MMNCFs and the comparable yield of $Lu_2ScN@C_{80}$ (I) and $LuSc_2N@C_{80}$ (I) is resulted from the much smaller difference on the ionic radius between Lu and Sc.

For $Lu_xSc_{3-x}N@C_{80}$ (II), the relative yields of $Lu_3N@C_{80}$ (II):$Lu_2ScN@C_{80}$ (II):$LuSc_2N@C_{80}$ (II):$Sc_3N@C_{80}$ (II) are calculated in the same way to be ca. 1:1.2:2.1:1.7 (see Supporting Information S2). Interestingly, the yield of $Lu_2ScN@C_{80}$

(II) and $LuSc_2N@C_{80}$ (II) is 1.2 and 2.1 times, respectively, of that of $Lu_3N@C_{80}$ (II), but only $LuSc_2N@C_{80}$ (II) surpasses $Sc_3N@C_{80}$ (II) in the yield while the yield of $Lu_2ScN@C_{80}$ (II) is 0.7 times of that of $Sc_3N@C_{80}$ (II). Again, this result is different from the case of $Gd_xSc_{3-x}N@C_{80}$ (II) for which the yield of both $Gd_2ScN@C_{80}$ (II) and $GdSc_2N@C_{80}$ (II) are obviously lower than that of $Sc_3N@C_{80}$ (II).[7] These results indicate that the formation of MMNCFs is sensitively dependent on the difference of the size of the two encaged metals, the composition of the mixed metal nitride (x value) and the isomeric structures of the carbon cage. If two metals with a relatively smaller difference in the ionic radius are mixed (e.g. Lu and Sc), they become more competitive during the formation of MMNCFs and the ratio of the yields is more close to the statistical distribution while Sc would generally dominate the formation of MMNCFs if a much larger metal atom such as Gd is mixed with Sc.

Electronic absorption spectra of the isolated $Lu_xSc_{3-x}N@C_{80}$ (I, II, x=1, 2): The UV-vis-NIR spectra of the isolated $Lu_xSc_{3-x}N@C_{80}$ (I, II, x=1, 2) dissolved in toluene are presented in Figure 3 in comparison with those of $Lu_3N@C_{80}$ (I) and $Sc_3N@C_{80}$ (I, II)[21] and their characteristic absorption data summarized in Table 1. For $Lu_xSc_{3-x}N@C_{80}$ (I), the main difference of their electronic spectra appears in the range of 600 – 700 nm, where $Lu_xSc_{3-x}N@C_{80}$ (I, x=1, 2) exhibit intermediate electronic absorption properties in comparison with $Lu_3N@C_{80}$ (I) and $Sc_3N@C_{80}$ (I). For instance, the overall absorption feature of $Lu_3N@C_{80}$ (I) is largely preserved in $Lu_2ScN@C_{80}$ (I) and $LuSc_2N@C_{80}$ (I) while the doublet peak with absorption maxima at 686/659 nm observed in the spectrum of $Lu_3N@C_{80}$ (I) is slightly red-shifted to 691/666 nm in $Lu_2ScN@C_{80}$ (I) and 706/685 nm in $LuSc_2N@C_{80}$ (I). However, in $Sc_3N@C_{80}$ (I) this feature is dramatically changed to a broad single band with absorption maximum at 735 nm (see inset of Figure 3a and Table 1). At the higher energy range, the strongest visible absorption peak at 403 nm in

the spectrum of $Lu_3N@C_{80}$ (I) keeps almost unchanged in $Lu_2ScN@C_{80}$ (I) while red-shifted in those of $LuSc_2N@C_{80}$ (I) and $Sc_3N@C_{80}$ (I)**.** The shoulder peak at 554 nm of $Lu_3N@C_{80}$ (I) (558 nm of $Lu_2ScN@C_{80}$ (I)) disappear in $LuSc_2N@C_{80}$ (I) and $Sc_3N@C_{80}$ (I) (see Figure 3a).

On the other hand, the electronic absorption spectra of $Lu_xSc_{3-x}N@C_{80}$ (II) are clearly different from those of the isomer I, which is consistent with the differences in the absorption spectra of the isomers I and II found earlier for homogeneous NCFs.[1,2,5a-b,7] With the variation of the $Lu_xSc_{3-x}N$ cluster composition, a significant change of the electronic spectrum occurs in $Lu_xSc_{3-x}N@C_{80}$ (II) (Figure 3b). For instance, the absorption peak at 714 nm observed in the spectrum of $Lu_2ScN@C_{80}$ (II) is red-shifted to ca. 727 nm of $LuSc_2N@C_{80}$ (II) and turns out to be nondetectable in $Sc_3N@C_{80}$ (II) (see inset of Figure 3b). Moreover, the shoulder peak at 631 nm in the spectrum of $Lu_2ScN@C_{80}$ (II) keeps almost unchanged in $LuSc_2N@C_{80}$ (II), while the strongest absorption peak in the visible range of $Lu_2ScN@C_{80}$ (II) at 463 nm splits into a doublet peak with absorption maxima at 414/455 nm in the spectrum of $LuSc_2N@C_{80}$ (II) (413/472 nm for $Sc_3N@C_{80}$ (II))**.** In this sense the overall absorption spectrum of $LuSc_2N@C_{80}$ (II) exhibits an intermediate feature in comparison with $Lu_2ScN@C_{80}$ (II) and $Sc_3N@C_{80}$ (II) with a higher resemblance to $Sc_3N@C_{80}$ (II).

Regardless of the difference in the electronic absorption features of $Lu_xSc_{3-x}N@C_{80}$ (I, II) (x=0-3), their optical band-gaps, derived from the absorption spectral onsets,[1-3,5,7-9,17,18] are quite close for the same isomeric structure (i.e. 1.51-1.57 eV for isomer I and 1.25-1.30 eV for isomer II, see Table 1).

FTIR vibrational spectra of the $Lu_xSc_{3-x}N@C_{80}$ (I, II, x=1, 2): The FTIR spectra of $Lu_xSc_{3-x}N@C_{80}$ (I) (x=0-3) are compared in Figure 4a. Clearly the cage vibrational modes (tangential (1100-1600 cm^{-1}) and radial modes (around 500 cm^{-1})[1,2,4,5,7-9,17,18,22]) of the four NCFs are identical, enabling us to assign the same cage isomer — C_{80}:7 with I_h symmetry[23] — to the carbon cages of $Lu_2ScN@C_{80}$ (I) and $LuSc_2N@C_{80}$ (I). Likewise, based on the close resemblances observed for the FTIR spectra of $Lu_2ScN@C_{80}$ (II) and $LuSc_2N@C_{80}$ (II) to that of $Sc_3N@C_{80}$ (II) as shown in Figure 4b,[21] we conclude that the cages of $Lu_2ScN@C_{80}$ (II) and $LuSc_2N@C_{80}$ (II) have the same isomeric structure as that of the $Sc_3N@C_{80}$ (II), i.e., C_{80}:6 with D_{5h} symmetry (see Figure 9).[23]

Figure 4 also shows the dependence of the antisymmetric M-N stretching vibrational modes ($\nu_{M\text{-}N}$) of $Lu_xSc_{3-x}N@C_{80}$ (I, II) (x=0-3), which are the most intense IR bands in the range of 600-800 cm^{-1}, on the composition of the encaged $Lu_xSc_{3-x}N$ cluster (see also Table 1).[1,2,4,5,7-9,17,18,22] The antisymmetric Lu-N stretching vibrational modes in $Lu_3N@C_{80}$ (I) ($\nu_{Lu\text{-}N}$, 703/714 cm^{-1}) and in $Sc_3N@C_{80}$ (I) ($\nu_{Sc\text{-}N}$, 599 cm^{-1}) is found to be splitted for the $Lu_xSc_{3-x}N@C_{80}$ (I).[4,7,8] To assign the observed vibrational modes, we carried out DFT calculations, pointing to a decrease of $\nu_{Lu—N}$ from 714 cm^{-1} in $Lu_3N@C_{80}$ (I) to 668/680/699 cm^{-1} in $Lu_2ScN@C_{80}$ (I) and to 652 cm^{-1} in $LuSc_2N@C_{80}$ (I), while $\nu_{Sc—N}$ increases from 599 cm^{-1} in $Sc_3N@C_{80}$ (I) to 652 cm^{-1} in $LuSc_2N@C_{80}$ (I) and to 710 cm^{-1} in $Lu_2ScN@C_{80}$ (I).[18] A similar evolution of $\nu_{M—N}$ and $\nu_{Sc—N}$ was observed for other $M_xSc_{3-x}N@C_{80}$ (M=Gd, Y, Er).[2,7,8,13] The evolution of $\nu_{Lu—N}$ and $\nu_{Sc—N}$ with the change of $Lu_xSc_{3-x}N$ cluster structure within $Lu_xSc_{3-x}N@C_{80}$ (II) was studied in a similar way, revealing that $\nu_{Lu—N}$ decreases from 639/660/683 cm^{-1} in $Lu_2ScN@C_{80}$ (II) to 638/642 cm^{-1} in $LuSc_2N@C_{80}$ (II), while $\nu_{Sc—N}$ increases from

599 cm^{-1} in $Sc_3N@C_{80}$ (II) to 649 cm^{-1} in $LuSc_2N@C_{80}$ (II) and to 697 cm^{-1} in $Lu_2ScN@C_{80}$ (II).

Comparison of the electronic absorption and FTIR vibrational spectra of $Lu_xSc_{3-x}N@C_{80}$ (I, x=1, 2) with $M_xSc_{3-x}N@C_{80}$ (I, M=Er, Dy, Gd, Nd): Interestingly, the evolvements of the electronic absorption and of the vibrational spectra of $Lu_xSc_{3-x}N@C_{80}$ (I, x=1, 2) are different to those found for $Gd_xSc_{3-x}N@C_{80}$ (I) reported earlier,[7,8] suggesting the dependence of the electronic absorption and the vibrational properties of $M_xSc_{3-x}N@C_{80}$ (I) on the encaged metal. The electronic absorption and the FTIR vibrational spectra of a series of $M_xSc_{3-x}N@C_{80}$ (I, M=Lu, Er, Dy, Gd, Nd, x=1, 2) together with those of $Sc_3N@C_{80}$ (I) (Figures 5 and 6) give a quite similar overall absorption feature of $M_xSc_{3-x}N@C_{80}$ (I, M=Lu, Er, Dy, Gd, Nd) while a slight discrepancy in the region of 600-800 nm has been recognized. For $M_2ScN@C_{80}$ (I), the doublet peak with absorption maxima at 691/666 nm in $Lu_2ScN@C_{80}$ (I) is gradually red-shifted to 698/669 nm in $Er_2ScN@C_{80}$ (I), 707/674 nm in $Dy_2ScN@C_{80}$ (I), 703/672 nm in $Gd_2ScN@C_{80}$ (I), and 711/677 nm in $Nd_2ScN@C_{80}$ (I) (see inset of Figure 5a). The more dramatic shifts are also found in the absorption spectra of $MSc_2N@C_{80}$ (I): the absorption maxima at 706 nm in $LuSc_2N@C_{80}$ (I) is gradually red-shifted to 711 nm in $ErSc_2N@C_{80}$ (I), 715 nm in $DySc_2N@C_{80}$ (I), 712 nm in $GdSc_2N@C_{80}$ (I), and 718 nm in $NdSc_2N@C_{80}$ (I), whereas the absorption maxima at 685 nm in $LuSc_2N@C_{80}$ (I) exhibits blue-shifts to 682 nm in $ErSc_2N@C_{80}$ (I) and 680 nm in $DySc_2N@C_{80}$ (I). It disappears in $GdSc_2N@C_{80}$ (I) and $NdSc_2N@C_{80}$ (I) (see inset of Figure 5b). As already revealed in the previous studies on the homogenous NCFs $M_3N@C_{80}$ (I) (M=Y, Gd, Tb, Dy, Ho, Er, Tm), the ionic radius of the encaged metal and consequently the size of the encaged M_3N cluster was found to play a dominating role not only in the structure of the M_3N cluster in $M_3N@C_{80}$ (I) and the cluster-cage interaction but also in the yield and

cage size distribution of the $M_3N@C_{2n}$ NCFs.[4] Hence, the dependence of the electronic absorption property of $M_xSc_{3-x}N@C_{80}$ (I) MMNCFs on the encaged metal is believed to attribute to the same effect. The ionic radii of Sc^{3+} is 0.75 Å, significantly smaller than those of Lu^{3+} (0.85 Å), Er^{3+} (0.88 Å), Dy^{3+} (0.91 Å), Gd^{3+} (0.94 Å) and Nd^{3+} (0.995 Å).[19] If one or two Sc atoms within $Sc_3N@C_{80}$ (I) are replaced by another lanthanide metal atom M with the larger ionic radius (M=Lu, Er, Dy, Gd, Nd) to form $M_xSc_{3-x}N@C_{80}$ (I) MMNCFs, the sum yield of the $M_xSc_{3-x}N@C_{80}$ (I) decreases with the increase of the ionic radius of M as demonstrated in Figure 1 and so does the energy of π-π^* transitions for $M_xSc_{3-x}N@C_{80}$ (I) derived from the absorption maxima (see Supporting Information S3). The similarity on the overall absorption features of $M_xSc_{3-x}N@C_{80}$ (I) suggests that their electronic spectra are dominated by the C_{80} carbon cage, while the above-mentioned change upon varying the encaged $M_xSc_{3-x}N$ cluster indicates a significant perturbation of the C_{80} cage which is dependent on the size of the encaged metal.

Figure 6 compares the FTIR vibrational spectra of a series of $M_xSc_{3-x}N@C_{80}$ (I, M=Lu, Er, Dy, Gd, Nd, x=1, 2) as well as that of $Sc_3N@C_{80}$ (I). While the cage vibrational modes are identical for all MMNCFs, the main discrepancy among their spectra is in the region of 600-800 cm^{-1}, which is correlated to the antisymmetric M-N stretching vibrational modes (ν_{M-N}).[1,2,4] As described above, ν_{M-N} is generally splitted in $M_xSc_{3-x}N@C_{80}$ (I) and the high-frequency vibrational mode has been assigned to ν_{Sc-N}. For $M_2ScN@C_{80}$ (I), ν_{Sc-N} clearly increases from 599 cm^{-1} in $Sc_3N@C_{80}$ (I) to 710 cm^{-1} in $Lu_2ScN@C_{80}$ (I) and further to 725 cm^{-1} in $Er_2ScN@C_{80}$ (I), 737 cm^{-1} in $Dy_2ScN@C_{80}$ (I), 759 cm^{-1} in $Gd_2ScN@C_{80}$ (I), and 769 cm^{-1} in $Nd_2ScN@C_{80}$ (I) (see inset of Figure 6a). Other vibrational modes assigned to ν_{M-N} exhibit a less pronounced shift. Similar changes on ν_{Sc-N} and ν_{M-N} are also found for $MSc_2N@C_{80}$ (I). For instance,

$\nu_{Sc\text{-}N}$ of $Sc_3N@C_{80}$ (I) (599 cm^{-1}) shifts to 652 cm^{-1} in $LuSc_2N@C_{80}$ (I), 667 cm^{-1} in $ErSc_2N@C_{80}$ (I), 678 cm^{-1} in $DySc_2N@C_{80}$ (I), 694 cm^{-1} in $GdSc_2N@C_{80}$ (I), and 715 cm^{-1} in $NdSc_2N@C_{80}$ (I) (see inset of Figure 6b), whereas $\nu_{M\text{-}N}$ keeps almost unchanged.

In our previous studies on the vibrational properties of the homogenous NCFs $M_3N@C_{80}$ (I) (M=Y, Gd, Tb, Dy, Ho, Er, Tm), we concluded that $\nu_{M\text{-}N}$ is directly correlated with the structure of M_3N, which is strongly dependent on the cluster size (ionic radius of the metal).[4] As a result, the increase of the ionic radius of the metal from Tm to Gd, causes a decrease of $\nu_{M\text{-}N}$ from 710 cm^{-1} in $Tm_3N@C_{80}$ (I) to 657 cm^{-1} in $Gd_3N@C_{80}$ (I), resulting from a decrease of force-constant of M-N bonds.[4] Interestingly, when the encaged metal changes from Lu to Nd within $M_xSc_{3-x}N@C_{80}$ (I, M=Lu, Er, Dy, Gd, Nd), the decrease of $\nu_{M\text{-}N}$ appears much smaller than that found for homogenous NCFs $M_3N@C_{80}$ (I). On the other hand, for $M_2ScN@C_{80}$ (I) $\nu_{Sc\text{-}N}$ are found to increase linearly when the ionic radius of the encaged metal increases from 0.85 Å (Lu^{3+}) to 0.995 Å (Nd^{3+}), while an even better linearity is obtained for $\nu_{Sc\text{-}N}$ within $MSc_2N@C_{80}$ (I) with M changing from Sc to Lu and to Nd (see Supporting Information S3). These results indicate that the force-constant of Sc-N bond within $MxSc_{3-x}N@C_{80}$ (I) depends sensitively on the size of the encaged metal.

NMR studies and assignments of the cage structures of the $Lu_xSc_{3-x}N@C_{80}$ (I, II, x=1, 2): Figure 7 shows the 125 MHz ^{13}C NMR spectra of $Lu_xSc_{3-x}N@C_{80}$ (I, II, x=0-3) obtained at room temperature and their characteristic NMR shifts ($\delta(^{13}C)$) are summarized in Table 1. The ^{13}C NMR spectra of $Lu_2ScN@C_{80}$ (I) and $LuSc_2N@C_{80}$ (I) are almost identical to those of $Sc_3N@C_{80}$ (I) and $Lu_3N@C_{80}$ (I), exhibiting two narrow lines with $\delta(^{13}C)$ of 137-138 and 144-145 ppm, respectively (see Figure 6a and Table 1). The intensity ratio of these two lines is 1: 3, which is characteristic for NCFs with the

C_{80} (I_h) cage isomer.[1,3,11,12,18,24] On the other hand, for $Lu_2ScN@C_{80}$ (II) and $LuSc_2N@C_{80}$ (II), their ^{13}C NMR spectra exhibit six narrow lines with $\delta(^{13}C)$ between 134 and 149.5 ppm. Among them, two lines with $\delta(^{13}C)$ of 142.5-145 ppm have the twofold intensities of those of the other four lines (see Figure 6b and Table 1). Clearly the ^{13}C NMR spectra of $Lu_2ScN@C_{80}$ (II) and $LuSc_2N@C_{80}$ (II) are almost identical to that of $Sc_3N@C_{80}$ (II) for which the characteristic six NMR lines have been assigned to six non-equivalent types of carbon atoms within C_{80} (D_{5h}) cage isomer.[1,24] Noteworthy, the assignments of the C_{80}:I_h cage isomer to $Lu_xSc_{3-x}N@C_{80}$ (I) and the C_{80}:D_{5h} cage isomer to $Lu_xSc_{3-x}N@C_{80}$ (II) are consistent with that obtained from FTIR studies as discussed above. Interestingly, for both isomers of $Lu_xSc_{3-x}N@C_{80}$ $\delta(^{13}C)$ shows appreciable changes with the variation of the $Lu_xSc_{3-x}N$ cluster composition (x value) and this effect is discussed in detail in next section.

The ^{45}Sc NMR spectra of $Lu_xSc_{3-x}N@C_{80}$ (I, II) at room temperature presented in Figure 8 exhibit a single and symmetric peak for all six fullerenes (see Table 1), indicating the dynamic behavior of the Sc atoms encaged in the carbon cage. For $Lu_xSc_{3-x}N@C_{80}$ (I), the ^{45}Sc NMR peak of $Sc_3N@C_{80}$ (I) (199.5 ppm)[3] keeps almost constant in $Lu_2ScN@C_{80}$ (I) and slighty downshifts to 194.7 ppm in $LuSc_2N@C_{80}$ (I), whereas that of $Sc_3N@C_{80}$ (II) (211.7 ppm) is found to downshift in both $Lu_2ScN@C_{80}$ (II) and $LuSc_2N@C_{80}$ (II) (194.7 ppm). The constancy of the ^{45}Sc NMR shift upon varying the composition of the $Lu_xSc_{3-x}N$ cluster (x value) within both isomers suggests that the internal motion of the Sc and Lu atoms within $Lu_xSc_{3-x}N@C_{80}$ (I, II) keeps the average dynamic environment for the Sc atoms constant within the $Lu_xSc_{3-x}N$ cluster. However, comparing the ^{45}Sc NMR shift reported for $CeSc_2N@C_{80}$ (I) (257.3 ppm at 313 K),[12] that of $LuSc_2N@C_{80}$ (I) is significantly smaller, resulting from the strong influence of the unpaired f-electron of the Ce atom in $CeSc_2N@C_{80}$(I) MMNCFs.

DFT study on the effect of the composition of the $Lu_xSc_{3-x}N$ cluster on the ^{13}C NMR shifts of $Lu_xSc_{3-x}N@C_{80}$ (I, II, x=1, 2): To understand the changes of the ^{13}C NMR chemical shifts of $Lu_xSc_{3-x}N@C_{80}$ (I, II) with the variation of the $Lu_xSc_{3-x}N$ cluster composition (x value), we performed DFT calculations on $Lu_xSc_{3-x}N@C_{80}$ (I, II) in a way similar to what was reported for $Gd_xSc_{3-x}N@C_{80}$ (I, II) and $Lu_xY_{3-x}N@C_{80}$ (I).[7,8,18] For $Lu_xSc_{3-x}N@C_{80}$ (I, I_h) it is known for the C_{80}:I_h cage that there are two different types of carbon atoms — the pyrene-type carbon atoms (triple-hexagon junctions (THJs) correlated to $\delta(^{13}C)$ with a lower shift of 137-138 ppm) and the corannulene-type carbon atoms (pentagon/hexagon/hexagon junctions (PHHJs) correlated to $\delta(^{13}C)$ with a higher shift around 144 ppm).[3,11a,18] According to our recent systematic study on the correlation of $\delta(^{13}C)$ with a π-orbital axis vector (POAV) angle[25,26] for $Lu_xY_{3-x}N@C_{80}$ (I) and $Lu_xSc_{3-x}N@C_{80}$ (I), the downshift of $\delta(^{13}C)$ of $Lu_xSc_{3-x}N@C_{80}$ (I) with the increase of the cluster size from $LuSc_2N$ to Lu_2ScN and to Lu_3N has been interpreted as the result of the increase of the pyramidalization of the pyrene-type carbon atoms, which is probed by the increase of the average POAV angles of the THJs carbon atoms.[18] It is remarkable that such a simple model which does not take into account the possible difference of the degree of the electron transfer between encaged cluster and the cage could provide a perfect linear correlation between the averaged POAV angles and $\delta(^{13}C)$ chemical shifts.

We then focus on $Lu_xSc_{3-x}N@C_{80}$ (II) in the following discussion. Figure 9A-B shows the DFT-optimized structures (conformers) of $Lu_2ScN@C_{80}$ (II) and $LuSc_2N@C_{80}$ (II) with C_{80}:D_{5h} cage (see Supporting Information S4), which has six non-equivalent types of carbon atoms (labeled as **a** – **f**) as illustrated in Figure 9C. Accordingly, six lines in ^{13}C NMR spectra of $Lu_xSc_{3-x}N@C_{80}$ (II) are observed as discussed above and the

assignments of each NMR line to different type of carbon atoms within $Lu_xSc_{3-x}N@C_{80}$ (II) are summarized in Table 2 which also includes the calculated average POAV angles for different types of carbon atoms. Accordingly, the experimental ^{13}C chemical shifts (exp. $\delta(^{13}C)$) versus the averaged POAV angles of each type of carbon atoms within $Lu_xSc_{3-x}N@C_{80}$ (II, D_{5h}) are plotted in Figure 10 which also includes those of the $Lu_xSc_{3-x}N@C_{80}$ (I, I_h) isomers for comparison.[18] There is a good linear correlation between $\delta(^{13}C)$ and the averaged POAV angles for all the three $Lu_xSc_{3-x}N@C_{80}$ (II) (x=0-2) NCFs except the type "**c**" atoms which systematically deviate from the linear correlation found for atoms of other types. The reason for that is unknown yet. On the other hand, with the variation of the $Lu_xSc_{3-x}N$ cluster composition (x value) within $Lu_xSc_{3-x}N@C_{80}$ (II, x=0-2), for a given type of carbon atom the change of the $\delta(^{13}C)$ is not directly correlated with the change of its averaged POAV angle as found in the I_h isomer of $Lu_xSc_{3-x}N@C_{80}$.[18,27] This effect is not fully understood at present because of the limited data points and a more systematic study based on the D_{5h} isomers of other MMNCFs is needed which is underway.

Conclusion

For the first time we report the synthesis and isolation of two isomers of Lu/Sc MMNCFs $Lu_xSc_{3-x}N@C_{80}$ (x=1, 2). The yield of $Lu_xSc_{3-x}N@C_{80}$ (I, x=1,2) relative to the homogenous NCFs $Sc_3N@C_{80}$ (I) and $Lu_3N@C_{80}$ (I) is found to be 1:2.5:2.7:1.4 ($Lu_3N@C_{80}$: $Lu_2ScN@C_{80}$:$LuSc_2N@C_{80}$:$Sc_3N@C_{80}$), indicating the boosting effect of the yield of $Lu_xSc_{3-x}N@C_{80}$ (I) upon mixing Lu and Sc metals compared to the homogeneous Lu- and Sc-NCFs. With the yield of $Lu_3N@C_{80}$ (II):$Lu_2ScN@C_{80}$ (II):$LuSc_2N@C_{80}$ (II):$Sc_3N@C_{80}$ (II) being 1:1.2:2.1:1.7, it is obvious that only $LuSc_2N@C_{80}$ (II) surpasses $Sc_3N@C_{80}$ (II) in its yield while both $Lu_2ScN@C_{80}$ (II) and

$LuSc_2N@C_{80}$ (II) have higher yields than $Lu_3N@C_{80}$ (II). The UV-vis-NIR spectroscopic study of $Lu_xSc_{3-x}N@C_{80}$ (I, II, x=0-3) reveals that the overall absorption feature of $Lu_3N@C_{80}$ (I) is largely preserved in $Lu_2ScN@C_{80}$ (I) and $LuSc_2N@C_{80}$ (I), whereas a more significant change of the electronic spectrum with the variation of the $Lu_xSc_{3-x}N$ cluster composition is found in $Lu_xSc_{3-x}N@C_{80}$ (II). The FTIR vibrational spectroscopic study leads to the assignments of the I_h and D_{5h} isomeric cage structures to $Lu_xSc_{3-x}N@C_{80}$ (I) and $Lu_xSc_{3-x}N@C_{80}$ (II), respectively, and such assignments are further consolidated by the ^{13}C NMR spectroscopic characterizations. Furthermore, the ^{45}Sc NMR spectroscopic study of $Lu_xSc_{3-x}N@C_{80}$ (I, II) reveals the constancy of the ^{45}Sc NMR shift upon varying the composition of the $Lu_xSc_{3-x}N$ cluster (x value), suggesting that the average dynamic environment for the Sc atoms within the $Lu_xSc_{3-x}N$ cluster is constant. DFT calculations reveal that the downshift of $\delta(^{13}C)$ of $Lu_xSc_{3-x}N@C_{80}$ (I) with the increase of the cluster size from $LuSc_2N$ to Lu_2ScN and to Lu_3N is the result of the increase of the pyramidalization of the pyrene-type carbon atoms. However, for $Lu_xSc_{3-x}N@C_{80}$ (II) such a simple correlation between the shift of $\delta(^{13}C)$ and the change of the averaged POAV angles for a given type of carbon atom is not found.

The electronic absorption properties of $Lu_xSc_{3-x}N@C_{80}$ (I, I_h) as compared to $M_xSc_{3-x}N@C_{80}$ (I, I_h, M= Er, Dy, Gd, Nd) shows a similarity of their overall absorption features, suggesting that their electronic spectra are dominated by the features of the C_{80}:I_h carbon cage with the significant perturbation of the cage which is dependent on the size of the encaged metal within the $M_xSc_{3-x}N$ cluster. The comparison study on the FTIR vibrational properties of $Lu_xSc_{3-x}N@C_{80}$ (I) with other $M_xSc_{3-x}N@C_{80}$ (I, M= Er, Dy, Gd, Nd) indicates that the force-constant of Sc-N bond within $M_xSc_{3-x}N@C_{80}$ (I) depends sensitively on the size of the encaged metal as well. As the first systematic

comparative study of a series of MMNCFs, this study provides a new insight to the metal-dependent properties of NCFs.

Acknowledgements. We gratefully acknowledge Ms. J. Schubert for the synthesis of $Nd_xSc_{3-x}N@C_{80}$ (see J. Schubert, Praxissemesterarbeit, IFW Dresden/FH Zittau 2007) and the technical assistances of Ms. K. Leger, Ms. S. Schiemenz, and Mr. F. Ziegs (all IFW Dresden). S. Y. thanks the Startup funding for the "100 Talents Programme of CAS" (No. ZC9850290028) from University of Science and Technology of China (USTC) and A. P. thanks the financial support from DAAD and AvH.

Supporting Information Available: Isolation of $Lu_xSc_{3-x}N@C_{80}$ (I, II, x=1, 2), estimation of the relative yield of $Lu_xSc_{3-x}N@C_{80}$ (I, II, x=1, 2) to those of $Lu_3N@C_{80}$ and $Sc_3N@C_{80}$, comparison of the characteristic data of electronic absorption and FTIR vibrational frequency of $M_xSc_{3-x}N@C_{80}$ (I, M=Lu, Er, Dy, Gd, Nd), and DFT-optimized conformers of $Lu_2ScN@C_{80}$ (II, D_{5h}) and $LuSc_2N@C_{80}$ (II, D_{5h}) with the lowest energy. This material is available free of charge via the Internet at http://pubs.acs.org.

References and Notes

(1) For recent reviews, see a) Dunsch, L.; Yang, S. F. *Small*, **2007**, *3*, 1298-1320; b) Dunsch, L.; Yang, S. F. *Phys. Chem. Chem. Phys.* **2007**, *9*, 3067-3081.

(2) Dunsch, L.; Krause, M.; Noack, J.; Georgi, P. *J. Phys. Chem. Sol.* **2004**, *65*, 309-315.

(3) Stevenson, S.; Rice, G.; Glass, T.; Harich, K.; Cromer, F.; Jordan, M.R.; Craft, J.; Hajdu, E.; Bible, R.; Olmstead, M. M.; Maitra, K.; Fisher, A.J.; Balch, A.L.; Dorn, H.C. *Nature* **1999**, *401*, 55-57.

(4) Yang, S. F.; Troyanov, S.; Popov, A.; Krause, M.; Dunsch, L. *J. Am. Chem. Soc.* **2006**, *128,* 16733-16739.

(5) a) Yang, S. F.; Dunsch, L. *J. Phys. Chem. B* **2005**, *109*, 12320-12328; b) Yang, S. F.; Dunsch, L. *Chem. Eur. J.* **2006,** *12***,** 413-419; c) Yang, S. F.; Kalbac, M.; Popov, A.; Dunsch, L. *Chem. Eur. J.* **2006**, 12, 7856-7862; d) Yang, S. F.; Popov, A.; Dunsch, L. *Angew. Chem. Int. Ed.* **2007**, *46*, 1256-1259;

(6) Popov, A. A.; Dunsch, L. *J. Am. Chem. Soc.* **2007**, *129*, 11835-11849.

(7) Yang, S. F.; Popov, A.; Kalbac, M.; Dunsch, L. *Chem. Eur. J.* **2008**, *14*, 2084-2092.

(8) Yang, S. F.; Kalbac, M.; Popov, A.; Dunsch, L. *ChemPhysChem* **2006**, *7*, 1990-1995.

(9) Yang, S. F.; Popov, A.; Dunsch, L. *J. Phys. Chem. B* **2007**, *111*, 13659-13663.

(10) a) Olmstead, M. M.; de Bettencourt-Dias, A.; Duchamp, J. C.; Stevenson, S.; Dorn, H. C.; Balch, A. L. *J. Am. Chem. Soc.* **2000**, *122*, 12220-12226; b) Macfarlane, R. M.; Bethune, D. S.; Stevenson, S.; Dorn, H. C. *Chem. Phys. Lett.* **2001**, *343*, 229-234; c) Ioffe, I. N.; Ievlev, A. S.; Boltalina, O. V.; Sidorov, L. N.; Dorn, H. C.; Stevenson, S.; Rice, G. *Int. J. Mass. Spectrom* **2002**, *213*, 183-189.

(11) a) Iezzi, E. B.; Duchamp, J. C.; Fletcher, K. R.; Glass, T. E.; Dorn, H. C. *Nano Lett.* **2002**, *2*, 1187-1190; b) Stevenson, S.; Lee, H. M.; Olmstead, M. M.; Kozikowski, C.; Stevenson, P.; Balch, A. L. *Chem. Eur. J.* **2002**, *8*, 4528-4535.

(12) Wang, X. L.; Zuo, T. M.; Olmstead, M. M.; Duchamp, J. C.; Glass, T. E.; Cromer, F.; Balch, A. L.; Dorn, H. C. *J. Am. Chem. Soc.* **2006,** *128*, 8884-8889.

(13) Chen, N.; Fan, L.Z.; Tan, K.; Wu, Y.Q.; Shu, C.Y.; Lu, X.; Wang, C. R. *J. Phys. Chem. C* **2007**, *111*, 11823-11828.

(14) Chen, N.; Zhang, E.; Tan, K.; Wang, C. R.; Lu, X. *Org. Lett.* **2007**, *9*, 2011-2013.

(15) Stevenson, S.; Chancellor, C. J.; Lee, H. M.; Olmstead, M. M., Balch, A.L. *Inorg. Chem.* **2008**, *47*, 1420-1427.

(16) Chen, N.; Zhang, E. Y.; Wang, C. R. *J. Phys. Chem. B* **2006**, *110*, 13322-13325.

(17) Yang, S. F.; Popov, A.; Dunsch, L. *Chem. Commun.* **2008**, 2885-2887.

(18) Yang, S. F.; Popov, A.; Dunsch, L. *Angew. Chem. Int. Ed.* **2008**, *47*, 8196-8200.

(19) Greenwood, N. N.; Earnshaw, A. *Chemistry of the Elements*, Pergamon, Oxford, **1984.**

(20) Krause, M.; Dunsch, L. *Angew. Chem. Int. Ed.* **2005**, *44*, 1557-1560.

(21) The amount of the isolated $Lu_3N@C_{80}$ (II) was so far not sufficient for the spectroscopic studies and $Lu_3N@C_{80}$ (II) is not the focus of this work.

(22) Krause, M.; Kuzmany, H.; Georgi, P.; Dunsch, L.; Vietze, K.; Seifert, G. *J. Chem. Phys.* **2001**, *115*, 6596-6605.

(23) Fowler, P. W.; Manolopoulos, D. E. *An Atlas of Fullerenes*, Clarendon Press, Oxford, **1995.**

(24) Duchamp, J. C.; Demortier, A.; Fletcher, K. R.; Dorn, D.; Iezzi, E. B.; Glass, T.; Dorn, H. C. *Chem. Phys. Lett.* **2003**, *375*, 655-659.

(25) Heine, T.; Buhl, M.; Fowler, P. W.; Seifert, G. *Chem. Phys. Lett.* **2000**, *316*, 373-380.

(26) Sun, G. Y.; Kertesz, M. *J. Phys. Chem. A* **2001**, *105*, 5212-5220.

(27) That is to say, for instance, with the increase of the cluster size from Sc_3N to $LuSc_2N$ and to Lu_2ScN within $Lu_xSc_{3-x}N@C_{80}$ (II), the $\delta(^{13}C)$ correlated to the type "**f**" carbon atoms increases gradually from 134.00 to 134.85 and to 135.05 ppm, but the averaged POAV angle keeps almost unchanged (8.26→8.25→8.26 deg for Sc_3N→$LuSc_2N$→Lu_2ScN). The similar inconsistency is also found for the types "**a**" and "**e**" carbon atoms which exhibit more significant increases on the $\delta(^{13}C)$ and the averaged POAV angles (see Table 2).

Table 1. Characteristics of $Lu_xSc_{3-x}N@C_{80}$ (I, II) NCFs.

x	Product	UV-vis-NIR absorption peaks (nm)	Onset (nm)	Band-Gap [a] (eV)	ν_{Sc-N} [b] (cm^{-1})	ν_{Lu-N} [b] (cm^{-1})	^{13}C NMR shifts ($\delta(^{13}C)$, ppm)	cage sym-metry	^{45}Sc NMR shifts (ppm)
3	$Lu_3N@C_{80}$ (I)	403, 554, 626, 659, 686	792	1.57	-	703, 714	137.39, 144.02	7:I_h	-
2	$Lu_2ScN@C_{80}$ (I)	402, 558, 666, 691	820	1.53	710	668, 680, 699	137.12, 143.99	7:I_h	199.5
1	$LuSc_2N@C_{80}$ (I)	410, 685, 706	820	1.51	652 [c]	652 [c]	136.90, 143.99	7:I_h	194.7
0	$Sc_3N@C_{80}$ (I)	424, 735	820	1.51	599	-	136.87, 144.18	7:I_h	199.5
2	$Lu_2ScN@C_{80}$ (II)	463, 631, 714	992	1.25	697	639, 660, 683	135.05, 138.31, 138.43, 143.22, 144.84, 149.18	6:D_{5h}	194.7
1	$LuSc_2N@C_{80}$ (II)	414, 455, 632, 727	958	1.29	649	638, 642	134.85, 138.00, 138.76, 143.45, 144.34, 148.51	6:D_{5h}	194.7
0	$Sc_3N@C_{80}$ (II)	413, 472	950	1.30	595	-	134.00, 137.34, 138.10, 142.75, 143.85, 147.68	6:D_{5h}	211.7

[a] the band-gap is converted from the onset (band-gap (eV)≈1240/onset (nm)).

[b] ν_{M-N} represents the antisymmetric stretching vibrational frequency of M-N.

[c] The coincidence of $\nu_{Lu—N}$ and $\nu_{Sc—N}$ in $LuSc_2N@C_{80}$ (I) is accidental.

Table 2. Averaged POAV angles (deg) [a] and experimental ^{13}C chemical shifts ($\delta(^{13}C)$, ppm) of $Lu_xSc_{3-x}N@C_{80}$ (II, D_{5h}).

Type of carbon atoms [b]	$Sc_3N@C_{80}$ (II)		$LuSc_2N@C_{80}$ (II)		$Lu_2ScN@C_{80}$ (II)	
	POAV	$\delta(^{13}C)$	POAV	$\delta(^{13}C)$	POAV	$\delta(^{13}C)$
f	8.26	134.00	8.25	134.85	8.26	135.05
b	9.06	137.34	8.93	138.00	9.19	138.31
c	10.30	138.10	10.25	138.76	10.23	138.43
d	10.47	142.75	10.49	143.45	10.45	143.22
a	10.51	143.85	10.52	144.34	10.47	144.84
e	11.28	147.68	11.48	148.51	11.33	149.18

[a] Averaging of POAV angles for different structures (conformers) was performed by taking into account their relative energies computed at the PBE/TZ2P level.

[b] See Fig. 9c for the labeling of the different types of carbon atoms.

.

.

FIGURE CAPTIONS

Figure 1. a) Chromatogram of a $Lu_xSc_{3-x}N@C_{2n}$ fullerene extract mixture synthesized by the ''reactive gas atmosphere'' method in comparison with those of $Gd_xSc_{3-x}N@C_{2n}$, $Dy_xSc_{3-x}N@C_{2n}$, and $Lu_xY_{3-x}N@C_{2n}$ (linear combination of two 4.6 x 250 mm Buckyprep columns; flow rate 1.6 ml/min; injection volume 100 µl; toluene as eluent (mobile phase); 40°C). The inset shows the enlarged chromatographic region of 30-38 min. Fraction 1: $Sc_3N@C_{78}$ + $Lu_xSc_{3-x}N@C_{80}$ (I, x=1-3); 2: $Sc_3N@C_{80}$ (I) + $Lu_xSc_{3-x}N@C_{80}$ (II, x=0-3) (see Supporting Information S1).

Figure 2. Positive-ion LD-TOF mass spectra of the isolated $Lu_xSc_{3-x}N@C_{80}$ (I, II, x=0-3).

Figure 3. UV-vis-NIR spectra of $Lu_xSc_{3-x}N@C_{80}$ (I, x=0-3) (a) and $Lu_xSc_{3-x}N@C_{80}$ (II, x=0-2) (b) dissolved in toluene. The insets show the enlarged spectral region.

Figure 4. FTIR spectra of $Lu_xSc_{3-x}N@C_{80}$ (I, x=0-3) (a) and $Lu_xSc_{3-x}N@C_{80}$ (II, x=0-3) (b).

Figure 5. UV-vis-NIR spectra of $M_2ScN@C_{80}$ (I) (a) and $MSc_2N@C_{80}$ (II) (b) dissolved in toluene (M=Lu, Er, Dy, Gd, Nd) in comparison with that of $Sc_3N@C_{80}$ (I). The insets show the enlarged spectral region.

Figure 6. FTIR spectra of $M_2ScN@C_{80}$ (I) (a) and $MSc_2N@C_{80}$ (II) (b) (M=Lu, Er, Dy, Gd, Nd) in comparison with that of $Sc_3N@C_{80}$ (I). The insets show the enlarged spectral region of 800-560 cm^{-1}. The asterisks in the FTIR spectrum of $Er_2ScN@C_{80}$ (I) mark the impurity.

Figure 7. The 125 MHz ^{13}C NMR spectra of $Lu_xSc_{3-x}N@C_{80}$ (I, x=0-3) (a) and $Lu_xSc_{3-x}N@C_{80}$ (II, x=0-2) (b) in CS_2/d_6-Acetone at room temperature.

Figure 8. The 121.5 MHz ^{45}Sc NMR spectra of $Lu_xSc_{3-x}N@C_{80}$ (I) (a) and $Lu_xSc_{3-x}N@C_{80}$ (II) (b) in CS_2/d_6-Acetone at room temperature (x=0-2).

Figure 9. DFT-optimized structures of $Lu_2ScN@C_{80}$ (II, D_{5h}) (A) and $LuSc_2N@C_{80}$ (II, D_{5h}) (B) with the lowest energy. The structures are viewed along the C_5 axis of C_{80}:D_{5h} cage which is

perpendicular to the plane of the paper. The Lu, Sc, and N atoms are drawn in purple, red, and blue, respectively. (C) Labeling of six non-equivalent types of carbon atoms (**a**-**f**) in C_{80}:D_{5h} cage.

Figure 10. Experimental ^{13}C chemical shifts (exp. $\delta(^{13}C)$) versus the averaged POAV angles of types "**a**”-“**f**" carbon atoms within $Lu_xSc_{3-x}N@C_{80}$ (II, D_{5h}) (the labeling is based on Figure 9c). The linear fit (black line) is based on all data points of the types "**a, b, d, e, f**" atoms within $Lu_xSc_{3-x}N@C_{80}$ (II, D_{5h}) (R^2=0.97). For comparison those data for $Lu_xSc_{3-x}N@C_{80}$ (I, I_h, x=0-3) are also plotted with the same color (▲) for all four NCFs (x=0-3) for clarity (their data points almost overlap in the scale of the figure).

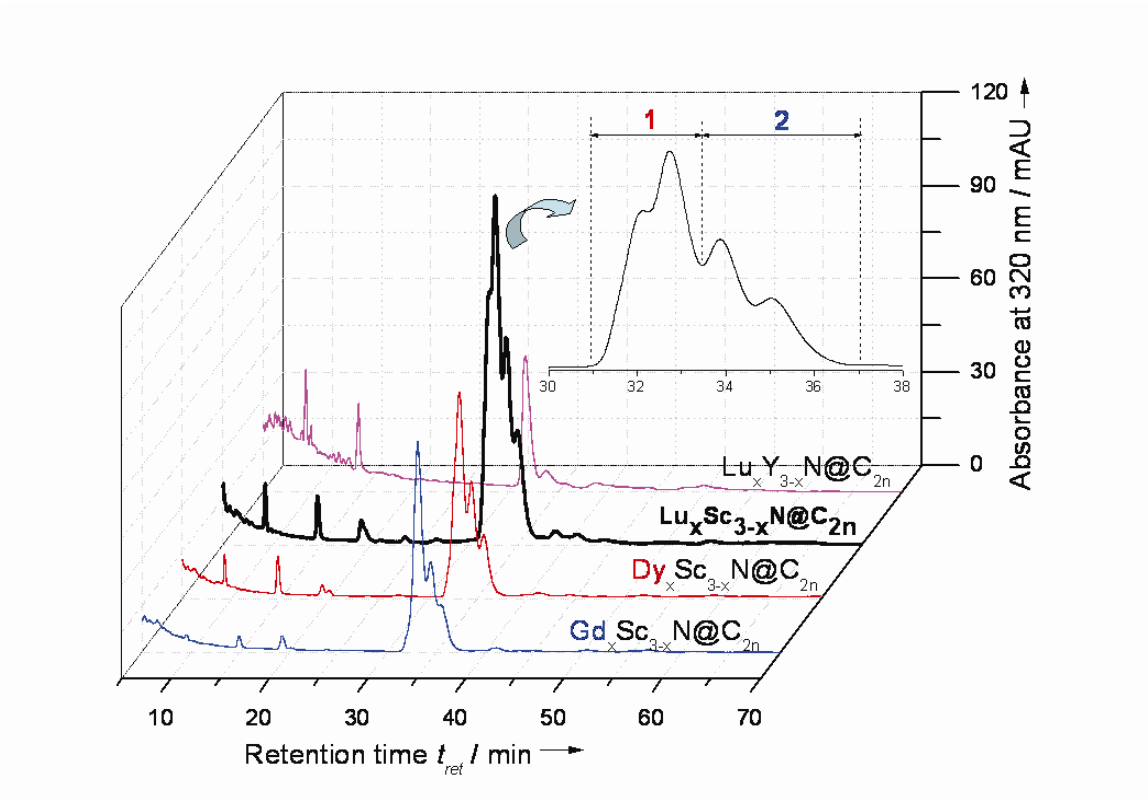
1
2
30
32
34
36
38
120
90
60
30
0
Absorbance at 320 nm / mAU
Lu$_x$Y$_{3-x}$N@C$_{2n}$
Lu$_x$Sc$_{3-x}$N@C$_{2n}$
Dy$_x$Sc$_{3-x}$N@C$_{2n}$
Gd$_x$Sc$_{3-x}$N@C$_{2n}$
10
20
30
40
50
60
70
Retention time t_{ret} / min

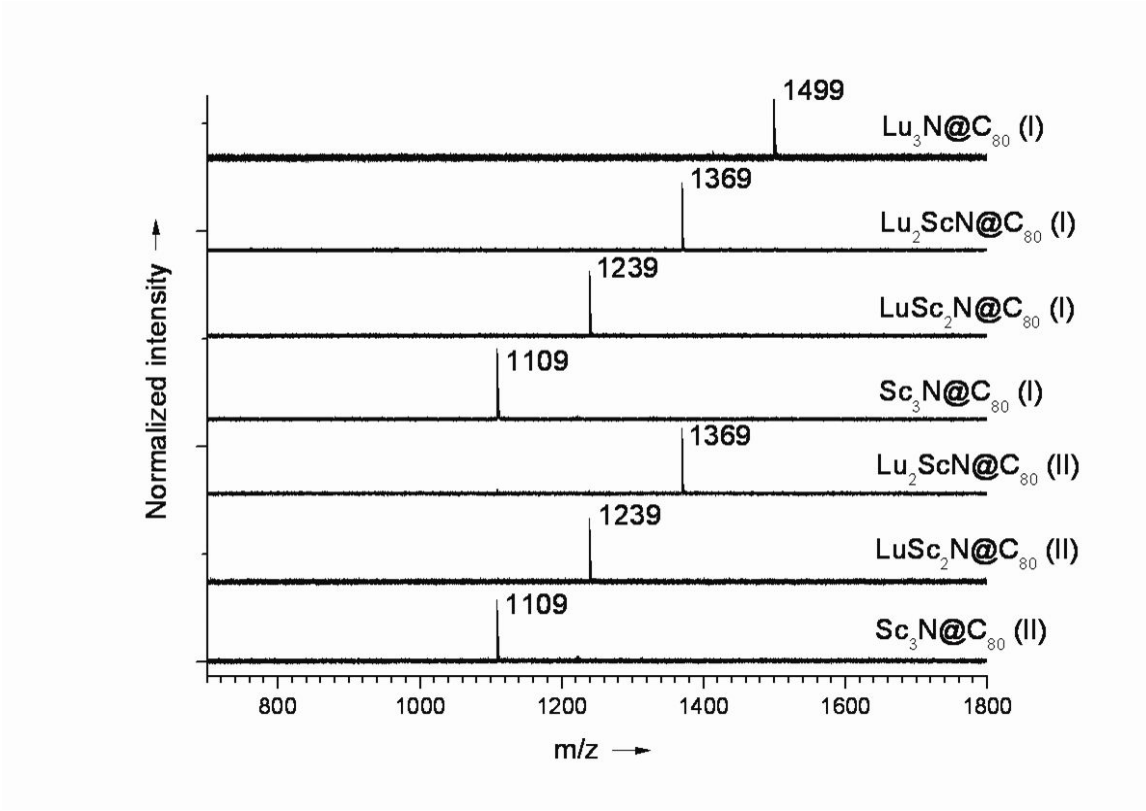
1499
Lu3N@C80 (I)
1369
Lu2ScN@C80 (I)
1239
LuSc2N@C80 (I)
1109
Sc3N@C80 (I)
1369
Lu2ScN@C80 (II)
1239
LuSc2N@C80 (II)
1109
Sc3N@C80 (II)
Normalized intensity
800
1000
1200
1400
1600
1800
m/z

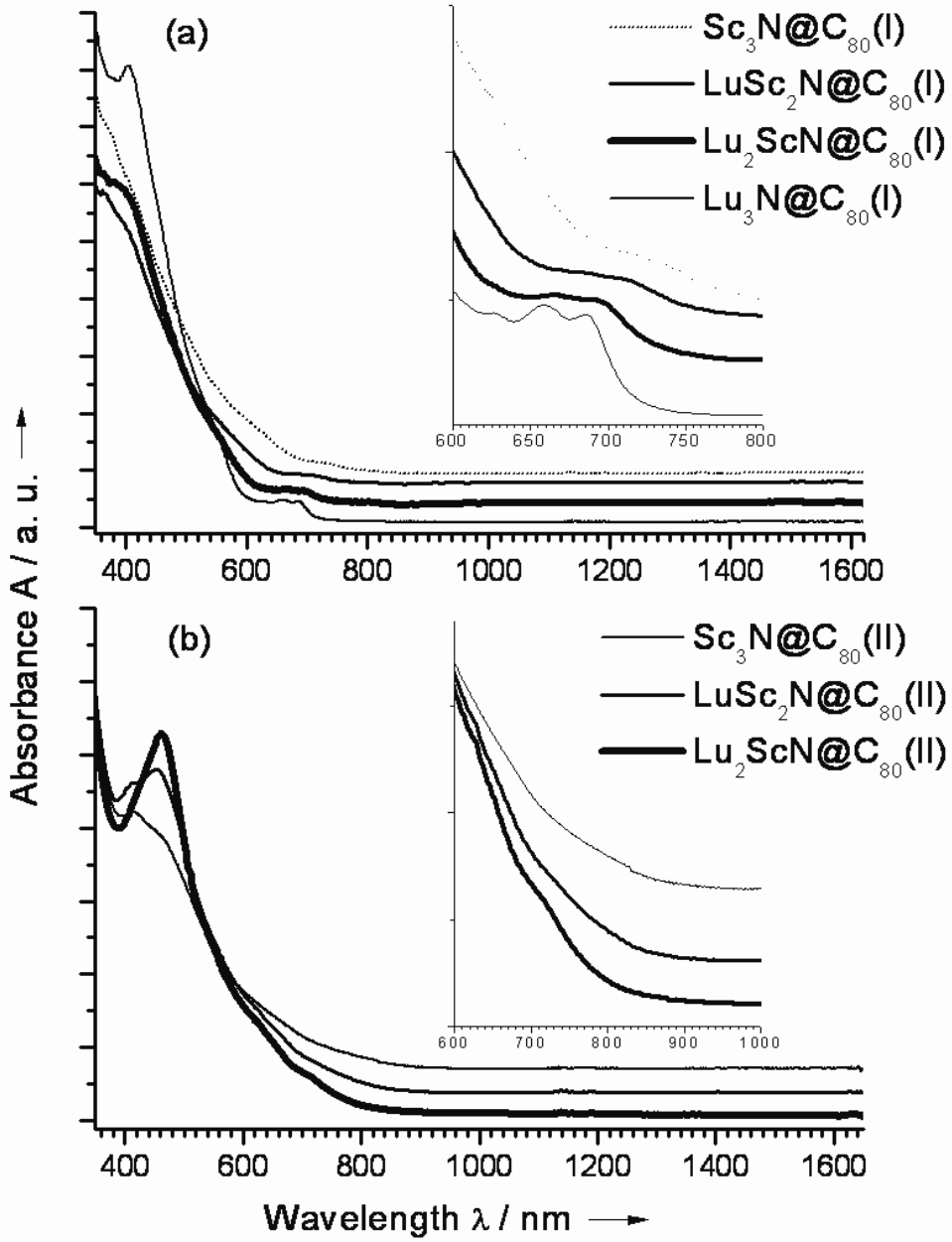
(a)
Sc3N@C80(I)
LuSc2N@C80(I)
Lu2ScN@C80(I)
Lu3N@C80(I)
600
650
700
750
800
400
600
800
1000
1200
1400
1600
(b)
Sc3N@C80(II)
LuSc2N@C80(II)
Lu2ScN@C80(II)
600
700
800
900
1000
400
600
800
1000
1200
1400
1600
Absorbance A / a. u.
Wavelength λ / nm

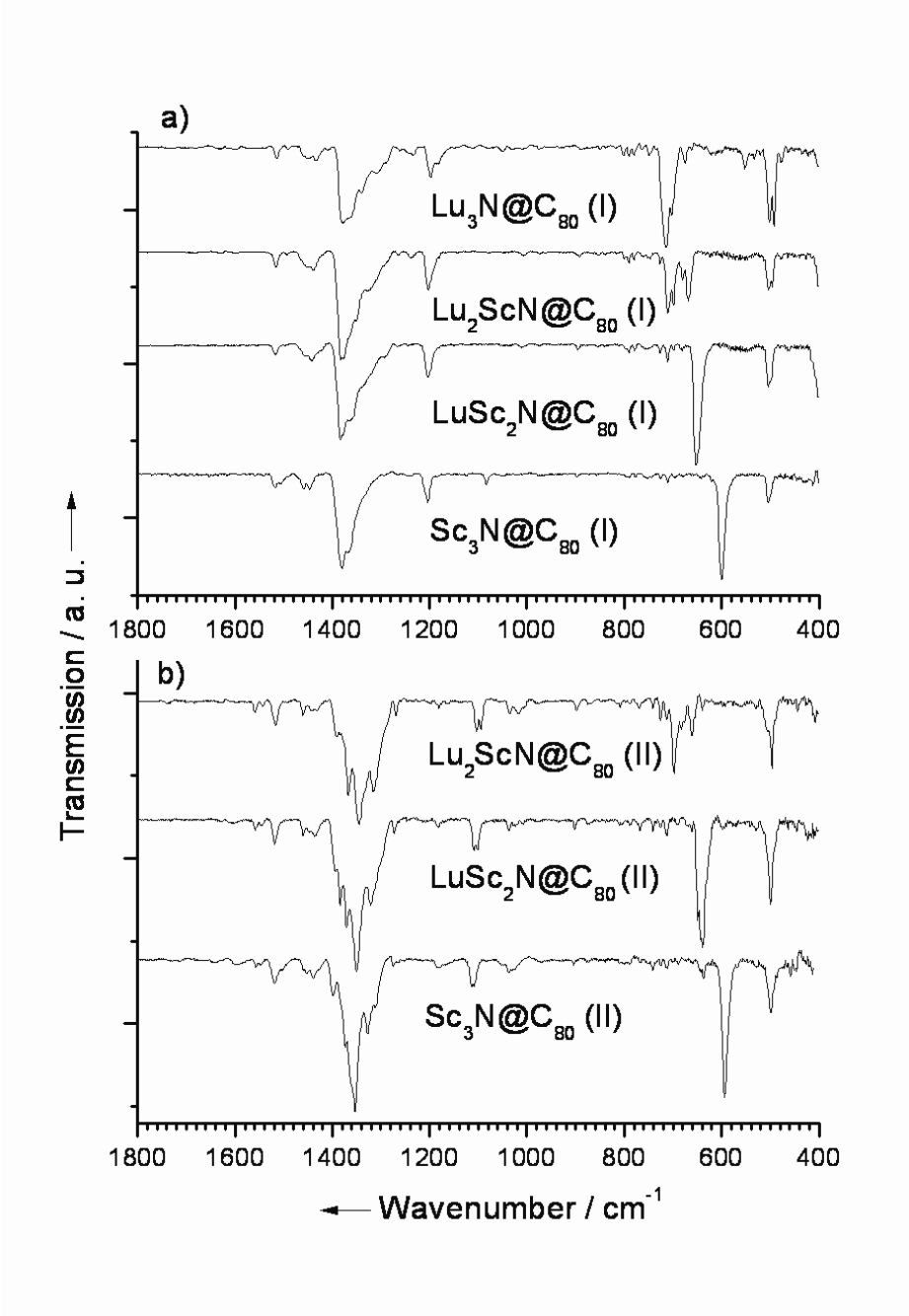
a)
Lu3N@C80 (I)
Lu2ScN@C80 (I)
LuSc2N@C80 (I)
Sc3N@C80 (I)
1800
1600
1400
1200
1000
800
600
400
b)
Lu2ScN@C80 (II)
LuSc2N@C80 (II)
Sc3N@C80 (II)
Transmission / a. u.
Wavenumber / cm-1

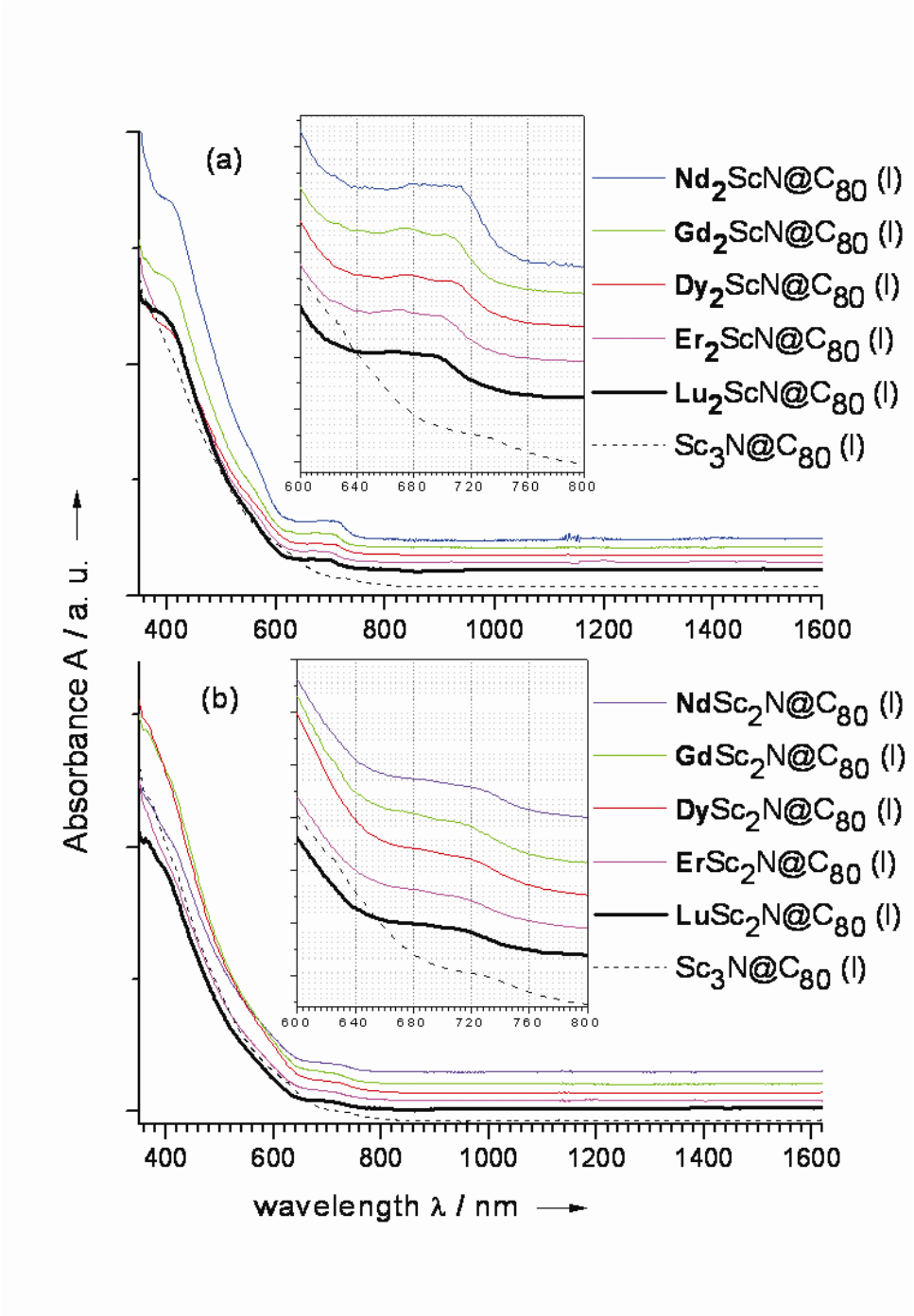
(a)
(b)
Absorbance A / a. u.
wavelength λ / nm
400
600
800
1000
1200
1400
1600
600
640
680
720
760
800
Nd2ScN@C80 (I)
Gd2ScN@C80 (I)
Dy2ScN@C80 (I)
Er2ScN@C80 (I)
Lu2ScN@C80 (I)
Sc3N@C80 (I)
NdSc2N@C80 (I)
GdSc2N@C80 (I)
DySc2N@C80 (I)
ErSc2N@C80 (I)
LuSc2N@C80 (I)
Sc3N@C80 (I)

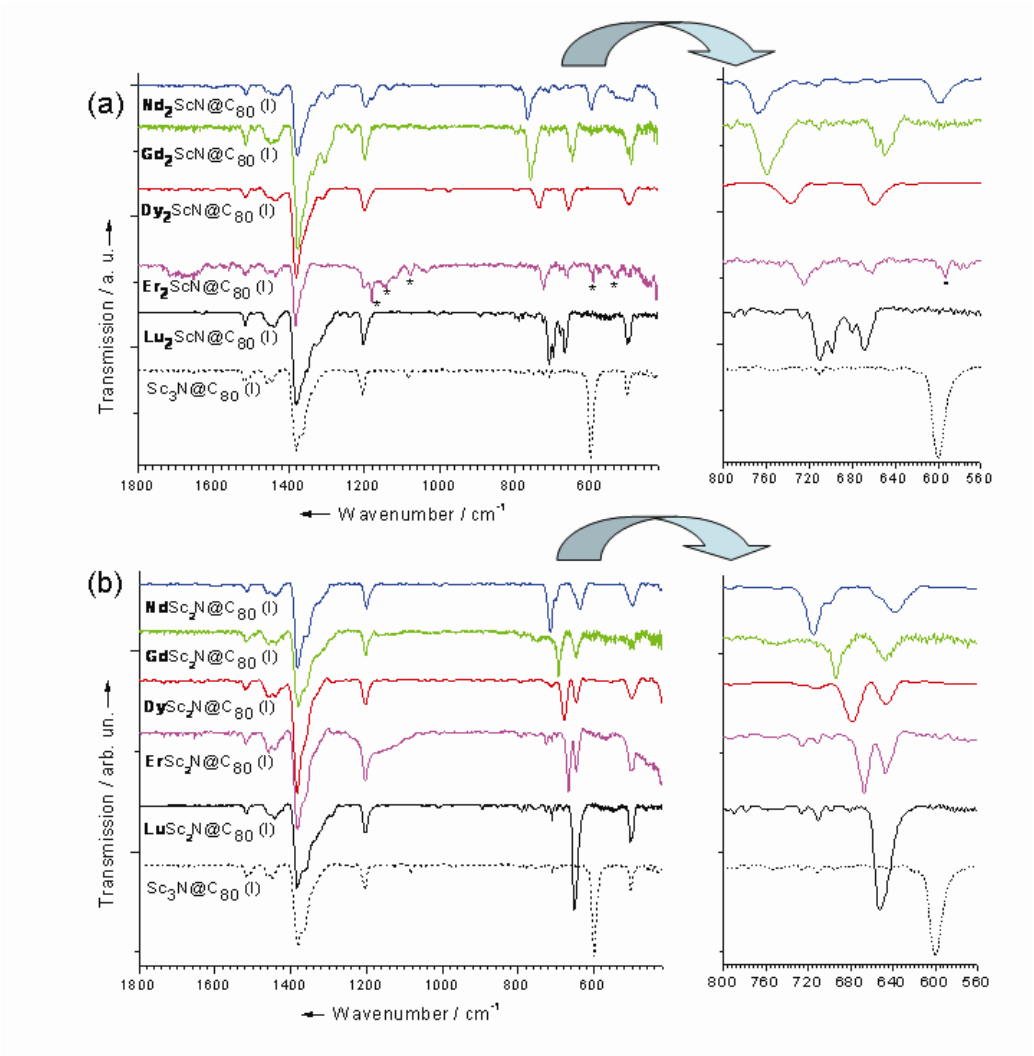
(a)
Nd2ScN@C80 (I)
Gd2ScN@C80 (I)
Dy2ScN@C80 (I)
Er2ScN@C80 (I)
Lu2ScN@C80 (I)
Sc3N@C80 (I)
Transmission / a. u.
1800 1600 1400 1200 1000 800 600
Wavenumber / cm-1
800 760 720 680 640 600 560
(b)
NdSc2N@C80 (I)
GdSc2N@C80 (I)
DySc2N@C80 (I)
ErSc2N@C80 (I)
LuSc2N@C80 (I)
Sc3N@C80 (I)
Transmission / arb. un.
1800 1600 1400 1200 1000 800 600
Wavenumber / cm-1
800 760 720 680 640 600 560

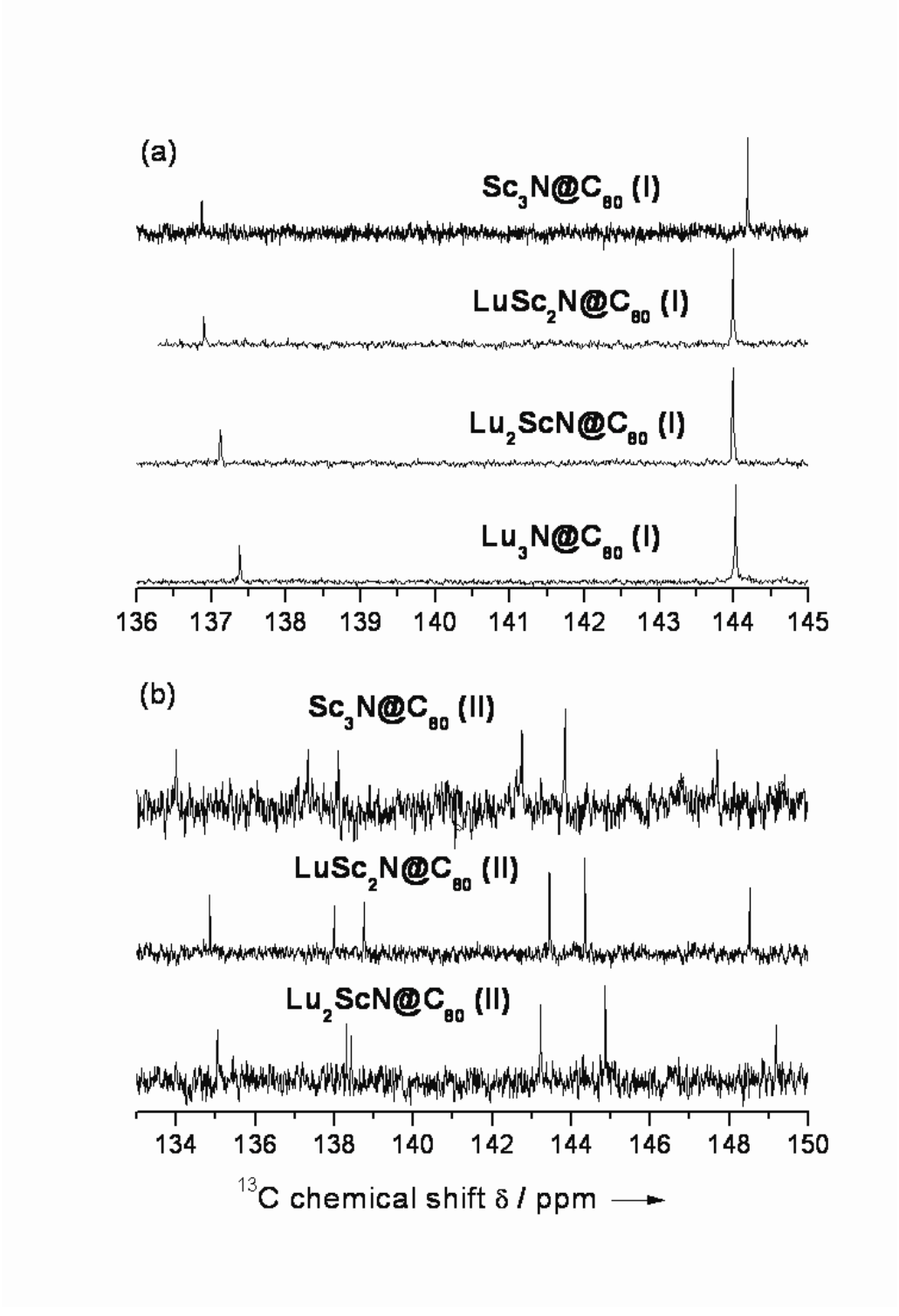
(a)
Sc3N@C80 (I)
LuSc2N@C80 (I)
Lu2ScN@C80 (I)
Lu3N@C80 (I)
136
137
138
139
140
141
142
143
144
145
(b)
Sc3N@C80 (II)
LuSc2N@C80 (II)
Lu2ScN@C80 (II)
134
136
138
140
142
144
146
148
150
13C chemical shift δ / ppm

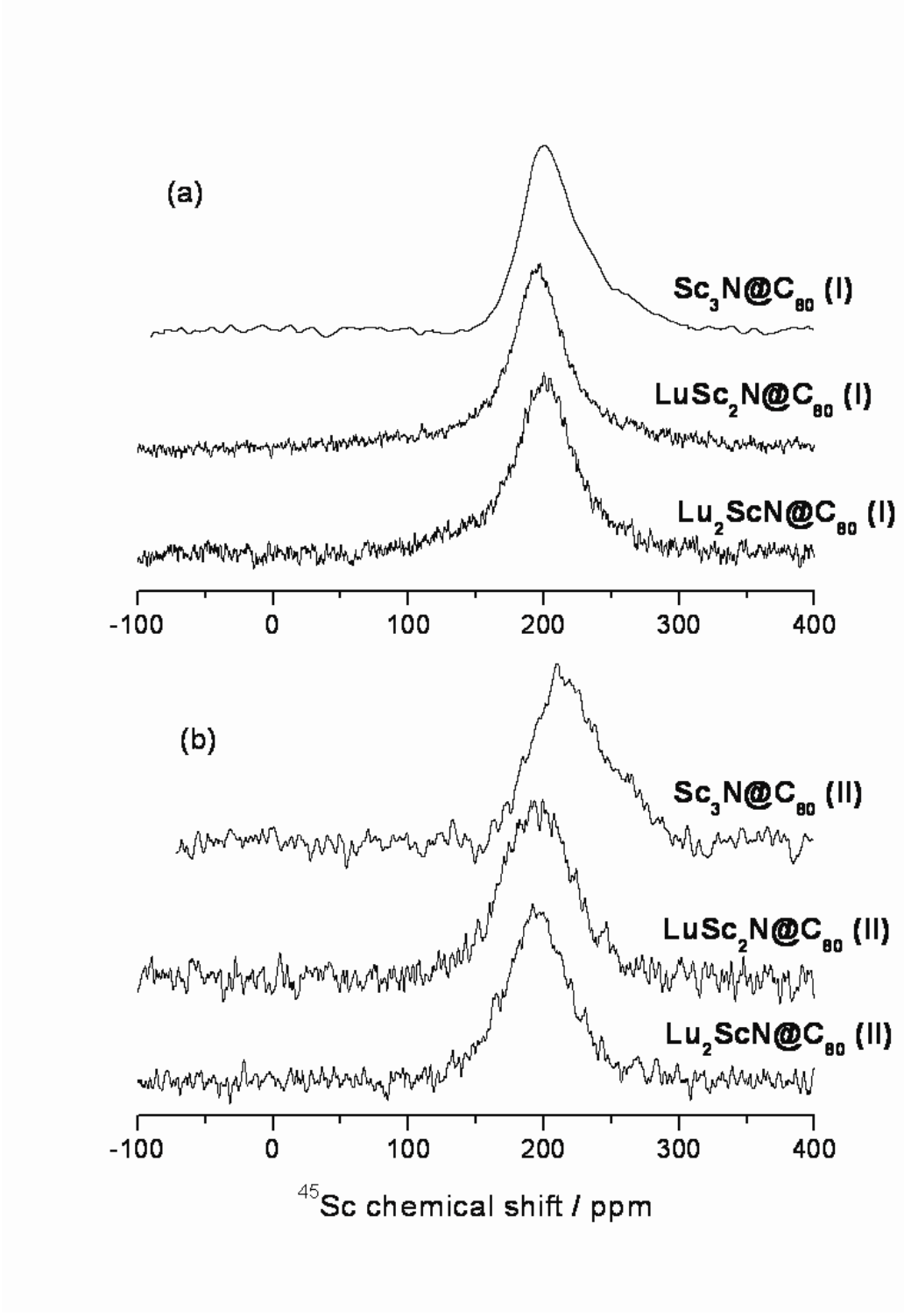
(a)
Sc3N@C80 (I)
LuSc2N@C80 (I)
Lu2ScN@C80 (I)
-100
0
100
200
300
400
(b)
Sc3N@C80 (II)
LuSc2N@C80 (II)
Lu2ScN@C80 (II)
-100
0
100
200
300
400
45Sc chemical shift / ppm

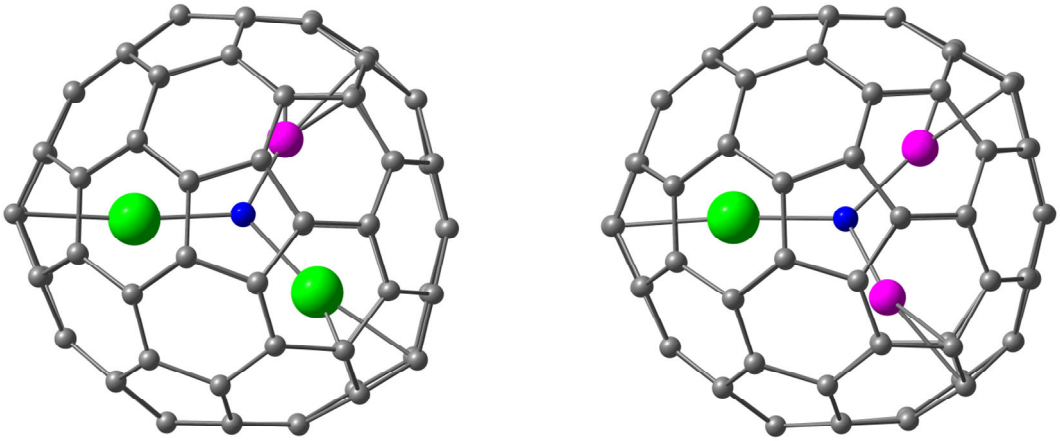

(A) (B)

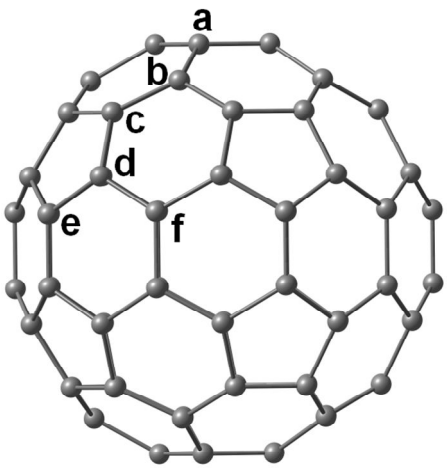

(C)

Yang, Popov, Chen, Dunsch, Figure 10

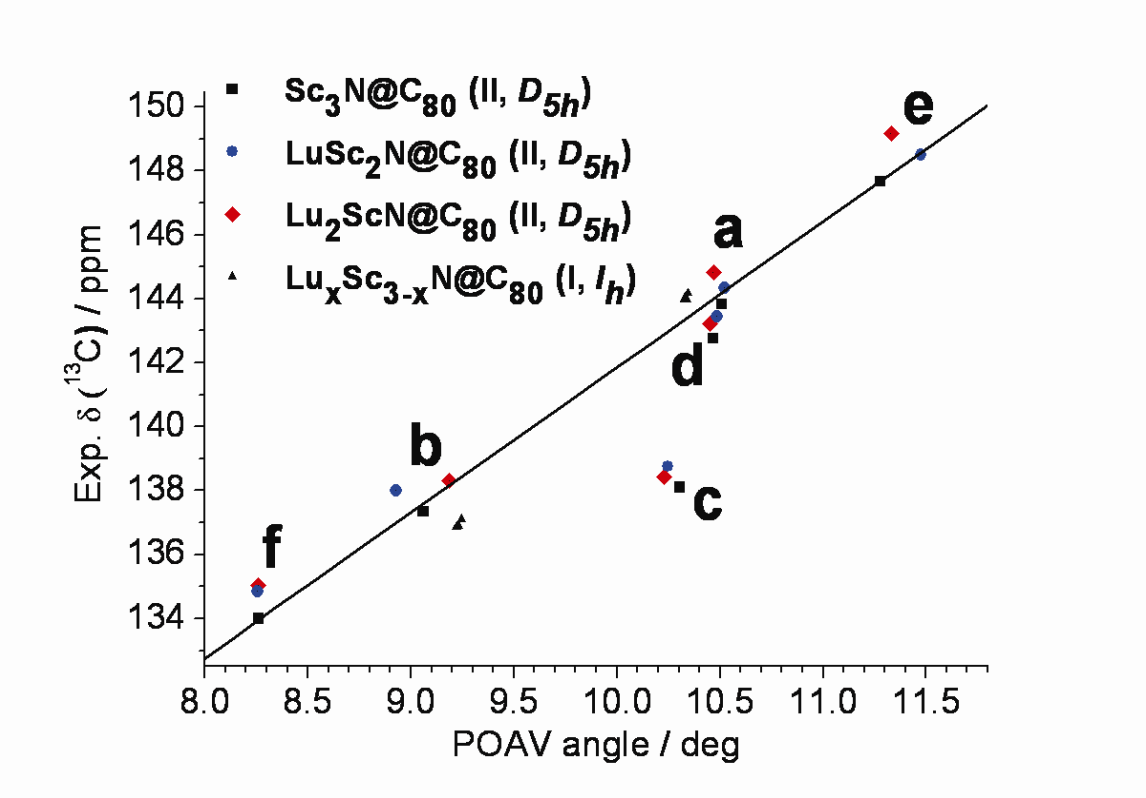

Mixed Metal Nitride Clusterfullerenes in Cage Isomers: $Lu_xSc_{3-x}N@C_{80}$ (x=1, 2) as Compared with $M_xSc_{3-x}N@C_{80}$ (M=Nd, Gd, Dy, Er)

Shangfeng Yang, Alexey Popov, Chuanbao Chen, and Lothar Dunsch